

High-temperature Creep Behavior of $\text{Al}_x\text{CrMnFeCoNi}$ High-entropy Alloys

C M Cao, J Xu, Y X Hao, W Tong and L M Peng*

CAS Key Laboratory of Mechanical Behavior and Design of Materials, Department of Modern Mechanics, School of Engineering Science, University of Science and Technology of China, Hefei, Anhui 230027, PR China

Corresponding author and email: L M Peng, penglm@ustc.edu.cn

Abstract. The creep deformation behavior of thermomechanically-treated $\text{Al}_x\text{CrMnFeCoNi}$ ($x=0.4$ and 0.6) high-entropy alloys was investigated under constant tensile loadings at 600-700 °C. It was found that the two alloys exhibited a mixed structure of fcc+bcc solid solutions with equiaxed grains and higher Al content produced a larger volume fraction of bcc phase. The double logarithmic plot of creep rate versus applied stress in $\text{Al}_{0.4}\text{CrMnFeCoNi}$ alloy was divided into two distinct regions with different stress exponents and activation energies depending on testing temperature and applied stress. In contrast, the $\text{Al}_{0.6}\text{CrMnFeCoNi}$ alloy exhibited a single value of stress exponent without transitional features. The $\text{Al}_{0.6}\text{CrMnFeCoNi}$ alloy showed lower creep resistance at a given stress and testing temperature compared to $\text{Al}_{0.4}\text{CrMnFeCoNi}$ alloy, which was ascribed to the higher stacking fault energy in the former alloy.

1. Introduction

Unlike traditional alloys that have one or two major metal elements, multi-component alloys or high entropy alloys (HEAs) contain at least five major elements with concentration range of 5-35 at% and have been an attractive subject as promising solid solution materials [1]. HEAs exhibit excellent mechanical properties such as excellent wear resistance, good corrosion resistance and high-temperature softening resistance [2-6]. The intrinsic mechanisms such as sluggish diffusion and lattice distortion for HEAs suggest an effective heat-resistance during plastic deformation process, especially under high-temperature performance. The single-fcc structured CoCrFeMnNi alloy has been widely investigated due to its excellent thermodynamic stability and high toughness especially in extreme low temperature [7]. Nevertheless, its strength and creep resistance needs to be further improved. One of the effective approaches is to introduce a certain amount of bcc solid solution into this alloy via adding other metal elements to obtain dual-phased microstructures. With this concept in mind, $(\text{FeCoNiCrMn})_{100-x}\text{Al}_x$ alloys were recently developed and their tensile properties in cast state were investigated at room temperature to examine the influence of microstructures [8]. Unfortunately, quite few reports have been available up to date on the high temperature creep deformation of these alloys.

Accordingly, the aim of present study is to investigate the tensile creep behavior of $\text{Al}_x\text{CrMnFeCoNi}$ high-entropy alloys. The stress exponent and activation energy for creep were

estimated based on the power-law creep equation to examine the corresponding mechanisms responsible for the creep deformation. The activation volume was determined to evaluate the effect of Al on the creep resistance and the creep fracture models were discussed based on SEM observations.

2. Experimental

The cast ingots with the nominal compositions of $\text{Al}_x\text{CrMnFeCoNi}$ ($x=0.4$ and 0.6 in molar ratio) were fabricated by vacuum-induction melting a mixture of six pure metals (all in high purity of 99.9 wt%) in a water-cooled copper crucible. All ingots were melted at least five times to ensure chemical homogeneity, and were drop-casted into a steel mold. The cast alloys were homogenized at $1150\text{ }^\circ\text{C}$ for 12 h in argon gas, and then rolled at $950\text{ }^\circ\text{C}$ to obtain a thickness reduction of 40%. The rolled plates were finally recrystallized at $1100\text{ }^\circ\text{C}$ for 2 h. Dog-bone shaped specimens with a gauge length of 25 mm were cut by electrical discharge machining. The tensile samples were tested on the CSS-3905 multi-functional machine under different loadings.

The crystalline structures of the samples were identified by X-ray diffraction (XRD) (PANalytical X'Pert Pro) with Cu-K_α radiation at 40 kV. The microstructures were observed using an optical microscope (OM) (AxiImager.Alm) and phase-compositional analysis were conducted using an energy dispersive spectroscope (EDS). For microstructural observation, samples were initially polished to 2500-grit SiC paper and, subsequently, etched with a solution composed of hydrogen peroxide and hydrochloric acid.

3. Results and discussions

3.1. Microstructures and XRD diffraction analysis

Figure 1 shows the microstructures and XRD patterns of $\text{Al}_x\text{CrMnFeCoNi}$ alloys (subsequently denoted as Al_x where $x=0.4$ or 0.6). Typical equiaxed grains and annealing twins are observed in the morphologies of these alloys. The bright and dark regions located at grain boundaries are identified as fcc and bcc phases, respectively. The volume fraction of bcc phase and the corresponding $(110)_{\text{bcc}}$ peak increase with the increase of Al concentration. The chemical compositions of phases measured by EDS are summarized in the Table 1. It is worth noting that Mn is homogeneously distributed in both fcc and bcc phases and bcc phase is enriched in Al and Ni, which is attributed to the mixing effect of enthalpies. The enthalpies of Cr-, Mn-, Fe-, Co- and Ni-Al are -10, -19, -11, -19 and -22 kJ/mol [9], respectively. Accordingly, Ni, not Cr and Fe tend to diffuse to bond with Al, leading to the formation of Ni-Al-rich bcc phase. In addition, the grain size of fcc phase for $\text{Al}_{0.6}$ is smaller compared to that of $\text{Al}_{0.4}$ as the grain-boundary bcc phases can hinder the growth of fcc phase.

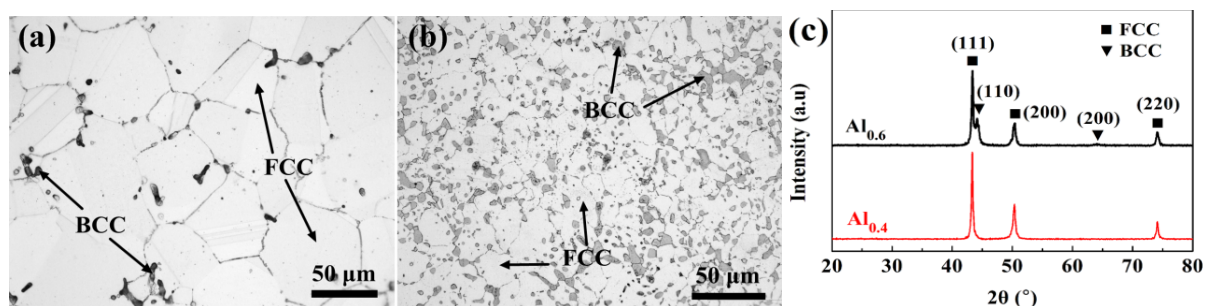


Figure 1. Microstructures of (a) $\text{Al}_{0.4}\text{CrMnFeCoNi}$ alloy and (b) $\text{Al}_{0.6}\text{CrMnFeCoNi}$ alloy, and (c) XRD patterns.

Table 1. Chemical compositions of Al_xHEAs obtained by EDS.

Alloys	Crystal	Chemical compositions/at. %					
		Al	Cr	Mn	Fe	Co	Ni
Al _{0.4}	Overall	6.42	19.50	18.72	18.81	17.58	18.97
	FCC	6.05	19.92	18.64	19.55	17.65	18.34
	BCC	22.95	6.00	18.15	7.41	12.02	33.48
Al _{0.6}	Overall	9.71	18.70	17.86	17.97	17.82	17.93
	FCC	6.89	20.81	18.06	20.00	18.66	15.59
	BCC	24.12	7.09	16.62	8.15	14.71	29.33

3.2 Creep deformation

Figure 2 exhibits the variations of creep strain and creep rate with testing temperature of Al_{0.4} and Al_{0.6} alloys at 650 °C. It is found that Al_{0.6} shows a higher creep rate than Al_{0.4} at a given temperature and stress. The creep deformation at the minimum creep rate held a short duration especially under higher applied stresses. In this case, the minimum creep rate is taken as the steady-state creep rate $\dot{\epsilon}$, and usually used to evaluate the creep behavior by correlating with the applied stress σ based on the Arrhenius-type equation [10]:

$$\dot{\epsilon} = A\sigma^n \exp\left(-\frac{Q}{RT}\right) \quad (1)$$

Where A is a material-dependent constant, σ is the applied stress, n is the stress exponent, and Q is the activation energy for creep deformation. As shown in Figure 3, the stress exponents were determined by plotting the variation of the steady-state creep rate with the applied stress on double logarithmic scales. It is found that the exponents of Al_{0.4} at 650 °C and 700 °C exhibit a stress-dependent transition with two distinct stress regions, i.e. low-stress region I with $n=1.6-2.2$ and high-stress region II with $n=4.2-4.9$, indicating a transition of rate-controlling mechanisms. In contrast, Al_{0.6} shows no transition in the stress exponents, with a single value of 5.8 at 600 and 2.8-3.5 at 650-700 °C.

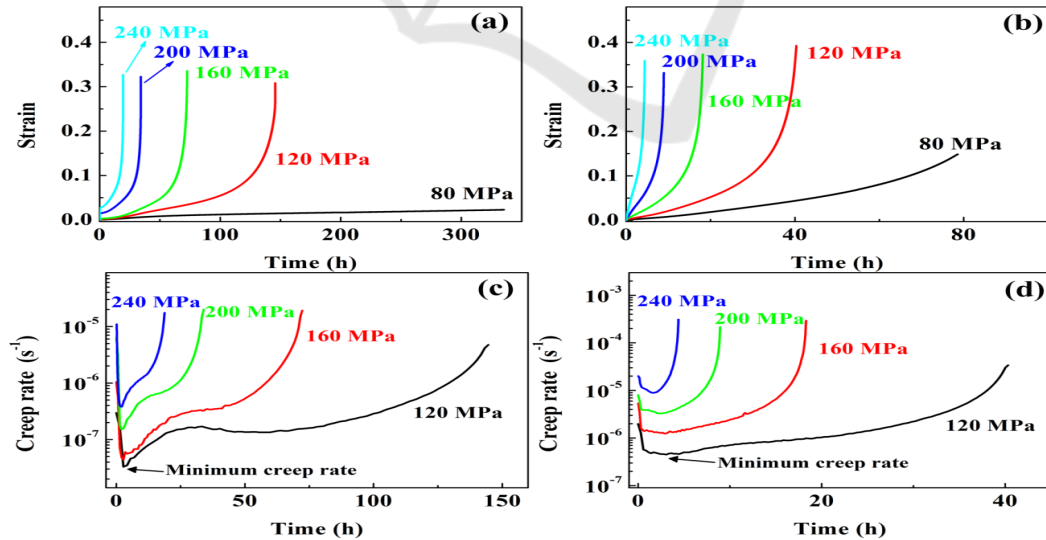


Figure 2. Creep curves at 650 °C for (a) Al_{0.4} and (b) Al_{0.6} alloys, and creep rate curves at 650 °C for (c) Al_{0.4} and (d) Al_{0.6} alloys at selected loadings.

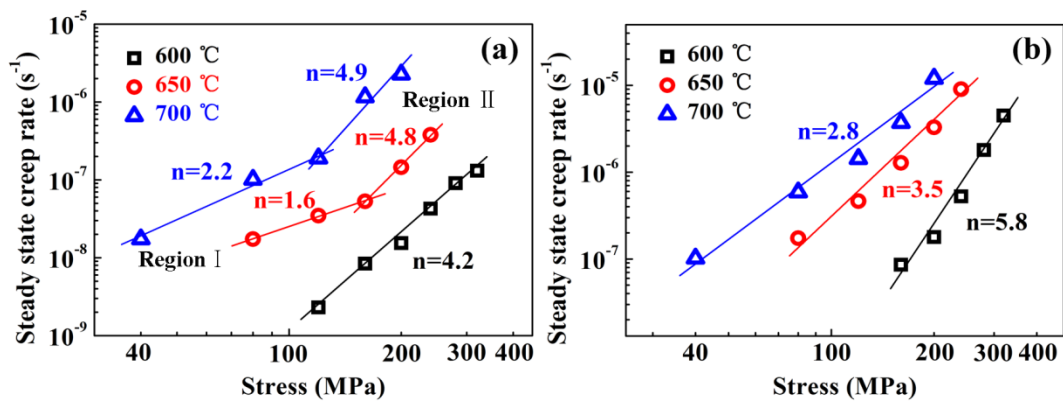


Figure 3. Steady state creep rate as a function of the applied stress on a double logarithmic plot for (a) $\text{Al}_{0.4}$ and (b) $\text{Al}_{0.6}$ alloys.

Based on equation (1), the activation energy was estimated by plotting the steady-state creep rate against $1/T$ at constant stresses on a semi-logarithmic scale as depicted in Figure 4. The average values of activation energy for region I and II are calculated as 258 and 349 kJ mol^{-1} , respectively, which are close to that of steady-state flow of FeCoNiCrMn alloy (284–333 kJ mol^{-1}) [10]. In contrast, the average activation energy at 650–700 °C is 188 kJ mol^{-1} .

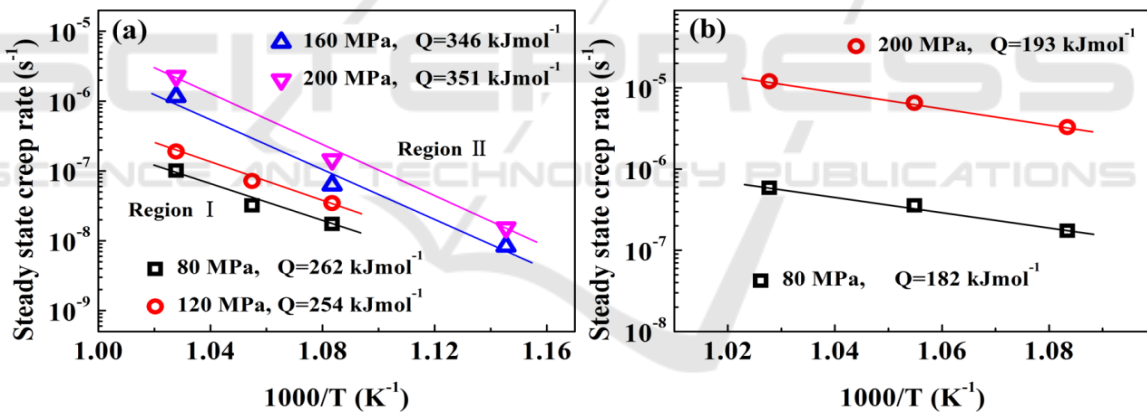


Figure 4. Arrhenius plot of steady-state creep rate versus temperature to determine the activation energy of (a) $\text{Al}_{0.4}\text{CrMnFeCoNi}$ alloy and (b) $\text{Al}_{0.6}\text{CrMnFeCoNi}$ alloy.

In general, it is difficult to determine which element is the contributing solute atom in the HEAs and the activation energies for lattice diffusion of constituent elements are not available. The activation energy of Al element is 126 kJ mol^{-1} , which is much lower than those for lattice diffusion of other constituent elements in the CrMnFeCoNi alloy (288–317 kJ mol^{-1}) [11,12]. Thus, it is reasonable to deduce that the creep deformation in these alloys is controlled by the five major elements with high activation energy. For $\text{Al}_{0.4}$ alloy, the creep mechanism of low-stress region is ascribed to the viscous glide of dislocations, which coincides with the previous research on the deformation mechanism with the stress exponent of 2 in FeCoNiCrMn alloy [10]. The activation energy of 258 kJ mol^{-1} is slightly lower than that of lattice diffusion of constituent elements in the CrMnFeCoNi alloy, suggesting that the creep rate is controlled by the diffusion of constituent elements as the solute atoms. In the region II, the stress exponent is close to 5, suggesting a

dislocation-climb mechanism. The larger activation energy of region II compared to that of region I is attributed to more constituent elements involved in solute atmosphere with the increase of stresses. The activation energy of 349 kJ mol⁻¹ for region II is close to that of lattice diffusion of Ni (317.5 kJ mol⁻¹), indicating that the creep rate is probably controlled by the sluggish diffusing species such as Ni. However, for Al_{0.6} tested under 650-700 °C, the activation energy of 188 kJ mol⁻¹ is much lower than that of major constituent elements. It is reported that the activation energy of pipe diffusion is a value around 0.4-0.7 times of the activation energy of lattice diffusion [13]. Considering the stress exponent of ~3, it can be inferred that the viscous glide of dislocations controlled by pipe diffusion is responsible for the creep mechanism in this region.

It is well known that the activation volume V^* as a common parameter can be employed to analyze the deformation mechanism. This parameter is defined as [14]

$$V^* = RT \frac{\partial \ln \dot{\epsilon}}{\partial \sigma} \quad (2)$$

where R represents the gas constant. The V^* values for Al_{0.4} are calculated as 1.40×10^{-4} , 1.48×10^{-4} and 2.03×10^{-4} m³ mol⁻¹ for 600 °C, 650 °C and 700 °C, respectively. For Al_{0.6}, V^* takes corresponding values of 1.80×10^{-4} , 1.89×10^{-4} and 2.41×10^{-4} m³ mol⁻¹. As a result, higher activation volume in the Al_{0.6} alloy causes a higher creep rate compared to Al_{0.4} under identical testing conditions. Similar feature have been verified in the previous investigation of the stress relaxation test on Al_xCoCrFeNi alloys [14].

3.3. Fractographs

Fracture morphologies of the two HEAs after creep rupture were presented in Figure 5. It was observed that the fractographs of Al_{0.4} exhibited typically ductile fracture with obvious dimples, whereas the fractographs of Al_{0.6} revealed a quasi-cleavage fracture mode characterized by cleavage surfaces and tearing ridges. It can be also noted that more oxides appear on the fracture surfaces subjected to long-term exposure at 700 °C.

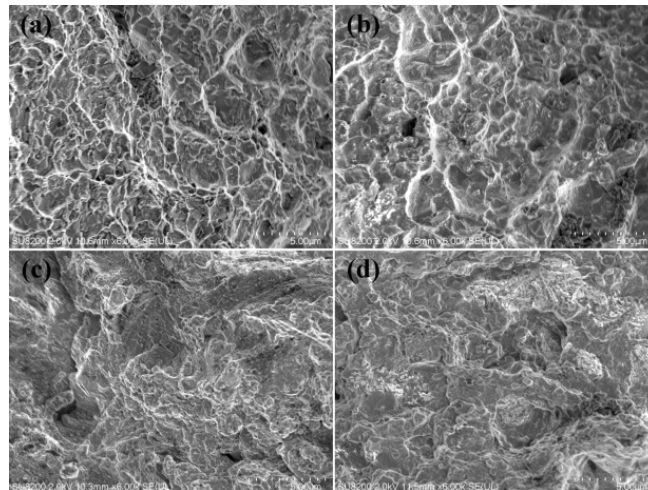


Figure 5. Fractographs of Al_{0.4}CrMnFeCoNi alloy crept at (a) 600 °C and (b) 700 °C, and Al_{0.6}CrMnFeCoNi alloy at (c) 600 °C and (d) 700 °C.

4. Conclusions

Two alloys showed equiaxed grains with fcc+bcc duplex structure, and higher Al content yields more volume of bcc phase and finer microstructure. Two creep-deformation regions for Al_{0.4} alloy are observed. In the low-stress region, the stress exponent is about 2 and the activation energy is 258 kJ mol⁻¹. The lattice diffusion controlled dislocation-glide mechanism is operative for the creep deformation. In contrast, the stress exponent of ~5 and the activation energy of 348 kJ mol⁻¹ indicate that lattice diffusion of sluggish diffusing species controlled dislocation-climb is responsible for the creep mechanism in the high-stress region. In the Al_{0.6} alloy, stress exponents are 5.8 at 600 °C and 3.2 at 650-700 °C. The calculated activation energy of 188 kJ mol⁻¹ at 650-700 °C implies that the creep deformation was dominated by dislocation glide controlled by pipe diffusion. In addition, the Al_{0.4}CrMnFeCoNi alloy with less stacking fault energy exhibits higher creep resistance compared to Al_{0.6}CrMnFeCoNi alloy. The investigated findings are important not only for understanding the tensile creep behavior of Al_xCrMnFeCoNi alloys, but also for future application of HEAs in high temperature.

Acknowledgements

This work was supported by the Natural Science Foundation of China (No. 11572306) and the Fundamental Research Funds for Central Universities (WK2090050040).

References

- [1] Yeh J W, Chen S K, Lin S J, Gan J Y, Chin T S, Shun T T, Tsau C H and Chang S Y 2004 *Adv. Eng. mater.* 6 299
- [2] Poletti M G, Fiore G, Gili F, Mangherini D and Battezzati L 2017 *Mater. Des.* 115 247
- [3] Gwalani B, Ayyagari A V, Choudhuri D, Scharf T, Mukherjee S, Gibson M and Banerjee R 2018 *Mater. Chem. Phys.* 210 197
- [4] Lin C M and Tsai H L 2011 *Intermetall.* 19 288
- [5] Chokshi A H 2018 *Mater. Chem. Phys.* 210 152
- [6] He J Y, Wang H, Wu Y, Liu X J, Nieh T G and Lu Z P 2017 *Mater. Sci. Eng. A.* 686 34
- [7] Otto F, Dlouhý A, Somsen C, Bei H, Eggeler G and George E P 2013 *Acta Mater.* 61 5743
- [8] He J Y, Liu W H, Wang H, Wu Y, Liu X J, Nieh T G and Lu Z P 2014 *Acta Mater.* 62 105
- [9] Takeuchi A and Inoue A 2005 *Mater. Trans.* 46 2817
- [10] He J Y, Zhu C, Zhou D Q, Liu W H, Nieh T G and Lu Z P 2014 *Intermetall.* 55 9
- [11] Edalati K and Horita Z 2011 *Scr. Mater.* 64 161
- [12] Tsai K Y, Tsai M H and Yeh J W 2013 *Acta Mater.* 61 4887
- [13] Fu J X, Cao C M, Tong W, Hao Y X and Peng L M 2017 *Mater. Sci. Eng. A.* 690 418
- [14] Cao T, Shang J, Zhao J, Cheng C, Wang R and Wang H 2016 *Mater. Lett.* 164 344